

## Article

# Influence of Triangle-Shaped Obstacles on the Energy and Exergy Performance of an Air-Cooled Photovoltaic Thermal (PVT) Collector

Byeong-Hwa An <sup>1</sup>, Kwang-Hwan Choi <sup>1</sup> and Hwi-Ung Choi <sup>2,\*</sup> 

<sup>1</sup> Department of Refrigeration and Air-Conditioning Engineering, Pukyong National University, Busan 48513, Korea

<sup>2</sup> Industry–University Cooperation Foundation, Pukyong National University, Busan 48513, Korea

\* Correspondence: nopoil@naver.com

**Abstract:** A photovoltaic thermal (PVT) collector is a type of solar collector that can simultaneously produce electrical and thermal energy from solar energy. In this research, the daily and annual performances of an air-cooled PVT collector with triangle-shaped obstacles were investigated and compared with those of a conventional air-cooled PVT collector. Based on the thermal circuit model, a numerical model of the air-cooled PVT collector containing triangle-shaped obstacles has been developed and validated using experimental results. A typical meteorological year's weather data from Ulsan, Korea was used as the weather data. From the results, it was seen that the daily average thermal, electrical, and overall energy and exergy efficiencies for the PVT collector with triangle-shaped obstacles were 24.73%, 15.59%, 62.83%, and 15.57%, respectively, while those values of conventional PVT collector were 17.08%, 15.30%, 54.47%, and 15.13%, respectively. The results also showed that the annual energy and exergy outputs of the PVT collector with triangle-shaped obstacles were 12.84% and 1.98% greater than those of the conventional air-cooled PVT collector. From these results, it was clearly confirmed that the triangle-shaped obstacles can enhance the energy and exergy outputs of the air-cooled PVT collector.

**Keywords:** photovoltaic thermal collector; solar thermal system; numerical analysis; energy efficiency; exergy



**Citation:** An, B.-H.; Choi, K.-H.; Choi, H.-U. Influence of Triangle-Shaped Obstacles on the Energy and Exergy Performance of an Air-Cooled Photovoltaic Thermal (PVT) Collector. *Sustainability* **2022**, *14*, 13233. <https://doi.org/10.3390/su142013233>

Academic Editors: Nuria Novas Castellano and Manuel Fernandez Ros

Received: 19 September 2022

Accepted: 13 October 2022

Published: 14 October 2022

**Publisher's Note:** MDPI stays neutral with regard to jurisdictional claims in published maps and institutional affiliations.



**Copyright:** © 2022 by the authors. Licensee MDPI, Basel, Switzerland. This article is an open access article distributed under the terms and conditions of the Creative Commons Attribution (CC BY) license (<https://creativecommons.org/licenses/by/4.0/>).

## 1. Introduction

In recent years, the photovoltaic (PV) module has become one of the most important renewable energy systems worldwide. This system directly converts solar radiation into electrical power and is widely used owing to its increase in efficiency with decreased cost. The disadvantage of PV modules is the high increase in temperature during the operation, which reduces their electrical efficiency. Wolf (1967) firstly suggested a hybrid photovoltaic thermal (PVT) collector to solve this problem [1]. The PVT collector combines a solar thermal collector with a PV module, making it capable of producing both electrical and thermal energy at the same time. In addition, because the cooling medium used in the solar thermal collector reduces the PV cell temperature, the electrical generation of the PV module can be improved.

Generally, liquid or air cooling is utilized to cool the PV cell in PVT collectors. PVT collectors with liquid cooling normally use liquids such as water or nanofluids. Many studies on water-based PVT collectors have aimed to confirm their thermal and electrical behaviors using experimental and numerical methods [2–7]. In addition, a number of studies have explored the use of nanofluids as heat transfer fluids to enrich the efficiency of liquid-cooled PVT collectors [8–12]. Liquid-cooled PVT collectors usually have higher efficiencies than air-cooled PVT collectors because the liquid's heat capacity and thermal conductivity are greater than those of air. However, owing to their relatively complex

design, liquid-cooled PVT collectors are more expensive and take up more space, and compared with air-cooled PVT collector, they are more difficult to install. In contrast, air-cooled PVT collectors have a simple design, are economical, and require little maintenance. Therefore, a great deal of research has been performed on increasing the thermal efficiency of air-cooled PVT collectors.

Changing the design parameters or configuration of an air-cooled PVT collector for enhanced thermal performance is one of the general methods to improve thermal performance. Sopian et al. compared an air-cooled PVT collector with a single-pass air channel to a collector with a double-pass air channel, and they found that the thermal and electrical efficiencies of the PVT air collector with a double-pass air channel varied between 32–34% and 8–9%, while the thermal and electrical efficiencies of the PVT air collector with a single-pass air channel varied between 24–28% and 6–7% under the similar conditions [13]. Agrawal and Tiwari proposed a PVT collector integrated with an additional micro-air channel; the exergy and energy performances of the collector was evaluated using a mathematical model [14]. The results indicated that the proposed PVT collector had greater annual energy and exergy gains than those of a conventional PVT collector, which has a single smooth air channel. Karima and Musafa compared four different PVT collectors experimentally and numerically. In this study, they found that the single-pass double-flow PVT collector produces higher thermal and electrical energy than those of other models [15]. Farshchimonfared et al. analyzed the effect of various design parameters on the performance of the PVT collector based on a thermal circuit model and reported that the optimum diameter of the air distribution duct and optimum depth of the air channel were 0.3–0.5 m and 0.09–0.026 m, respectively [16]. Slimani et al. mathematically modeled the PV module and three different PVT air collectors and compared their daily and annual energy performances [17]. As a result of this study, the glazed double-pass PVT collector was found to have the highest performance, with daily electrical, thermal, and overall efficiencies of 10.65%, 44.41%, and 74%, respectively, while the conventional unglazed collector had efficiencies of 10.73%, 21.19%, and 51.02%, respectively.

The other method of enhancing the thermal performance of the PVT collector is to use heat transfer enhancement devices to increase the heat transfer area. Jin et al. evaluated the performance of the PVT collector employing a rectangular tunnel absorber and concluded that the suggested system can produce improved thermal and electrical outputs [18]. Hussain et al. tested the electrical and thermal performance of the PVT collector incorporating a hexagonal honeycomb heat exchanger [19]. This study reported that the presence of the hexagonal honeycomb heat exchanger improved both the electrical and thermal outputs. Fudholi et al. conducted an experiment and theoretical analysis of a PVT collector with a del-groove heat exchanger under various solar intensity and air mass flow rate conditions [20]. The results showed that the energy and exergy performance of the proposed PVT collector varied between 38.8–81.8% and 12.44–13.26% depending on the operating conditions. Ahmad et al. conducted a numerical analysis to estimate electrical and cooling performance for the PV module with the newly suggested fin, and the results showed that the proposed fin reduces average cell temperature and improves electrical power output of the PV module by 2.87% [21]. In addition, a number of studies have been performed that have focused on either changing configuration of the PVT collector or using a heat transfer enhancement device that extends the heat transfer area [22–28].

Another method is installing obstacles in the air duct of the PVT collector. As fluid flows through a constricted area provided by an obstacle, its velocity increases, thereby improving the convective heat transfer coefficient in an air duct of the collector. The purpose of the obstacles is to provide better performance in heat transfer by generating an increase in local air velocity in an air duct separately from changing the configuration of the collector or extending the heat transfer area. Moreover, this method has benefits in manufacturing and price because of its simple design. Kim et al. proposed a PVT collector with a round heat-absorbing plate in an air channel and experimentally investigated its performance, and they reported that the suggested PVT collector had thermal and electrical efficiencies

of 29–42% and 15.71–16.25%, respectively [29]. Choi et al. evaluated the performance of a PVT collector coupled with a triangle-shaped obstacle located at the bottom of the air duct, experimentally, in the actual weather condition [30,31]. The results indicated that the proposed PVT collector exhibits thermal efficiency of 28.83–38.36% and electrical efficiency of 16.15–16.43%. Yu et al. suggested a PVT collector with a baffle at the base of an air duct and investigated its performance with various arrangements of the baffles through numerical simulation [32]. As a result, it was found that the baffles can improve the heat gain of the PVT collector by 1.28–1.31 times over a collector without baffles.

However, based on the above literature review, it was observed that only a few studies on the PVT collector coupled with obstacles have been performed in comparison with other methods. Additionally, energy and exergy improvement by the addition of obstacles have not yet been well discussed and assessed in the previous research, especially on a daily and annual basis. Thus, it will be interesting to confirm how much more energy and exergy can be achieved with the addition of the obstacle. Therefore, this study evaluated the energy and exergy performance of the PVT collector coupled with obstacles on a daily and annual basis. The triangle-shaped obstacle, which is easy to fabricate due to its simple design, was employed as an obstacle. The mathematical model of the PVT collector coupled with triangle-shaped obstacles was developed to estimate the performance of the collector and it was validated with experimental values reported in previous research [30]. Finally, by using the developed simulation model, this study examined how the obstacle installed in an air channel of the PVT collector affects its electrical and thermal behaviors, as well as evaluated energy and exergy improvement by the obstacle over daily and annual periods.

## 2. Mathematical Modeling

### 2.1. Theoretical Model of the Air-Cooled PVT Collector

Figure 1 presents a schematic of the conventional air-cooled PVT collector and the collector with triangle-shaped obstacles. Both PVT collectors are single-pass unglazed flat-plate air-cooled PVT collectors. In the present work, the PVT collectors with and without triangular obstacles are modeled based on the simple thermal circuit model reported and used in previous studies similar to the present work [16,33–36].

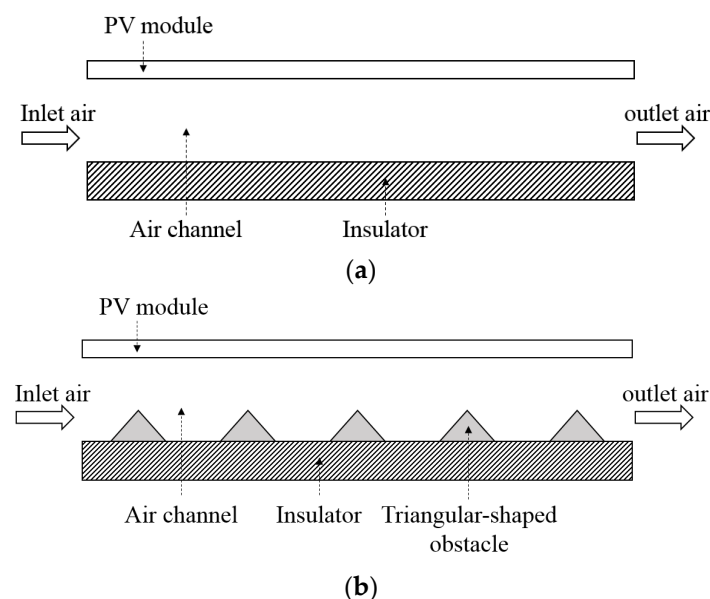


**Figure 1.** Schematic of the side views of air-cooled PVT collector (a) without triangle-shaped obstacles (conventional air-cooled PVT collector) and (b) with triangle-shaped obstacles.

To simplify the modeling of the air-cooled PVT collector, in this study, the following assumptions were taken into account:

- The PVT collector was assumed to be in a steady-state condition.
- Conduction heat transfer along the thickness of the solid layer was neglected due to their low thickness.
- The ambient air temperature was equal to the inlet air temperature of the collector.
- Since the side and bottom surfaces of the PVT collector were well insulated, heat loss at the side and bottom surfaces were ignored.
- The design parameters and properties of air were assumed to be constant.

Since the PVT collector was assumed in steady-state conditions, the energy balance in the PVT collector can be expressed as follows [16,33]:

$$G(\alpha - \eta_{el}) = \dot{q}_{th} + \dot{q}_{loss} \quad (1)$$

where  $\alpha$  is absorptivity of the PV module,  $\eta_{el}$  is electrical efficiency of PV module, and  $G$  is solar intensity. The left-hand side term in Equation (1) indicates the solar radiation absorbed by the PV module minus the electrical power output. The right-hand side terms involve heat gain of air ( $\dot{q}_{th}$ ) and heat loss at the collector's top surface ( $\dot{q}_{loss}$ ).

Based on the above Equation (1), the outlet air temperature ( $T_{air,out}$ ), thermal output of the PVT collector ( $\dot{q}_{th}$ ), thermal efficiency ( $\eta_{th}$ ), electrical power output ( $\dot{W}_{PV}$ ), and electrical efficiency ( $\eta_{el}$ ) for the thermal circuit model have been derived as follows [16,33]:

$$T_{air,out} = T_a + [T_{eff} - T_a + (\alpha - \eta_{el})GR_t] \left[ 1 - \exp\left(-\frac{A_c}{\dot{m}C_p R_{ov}}\right) \right] \quad (2)$$

$$\dot{q}_{th} = \frac{\dot{m}c_p}{A_c} [T_{eff} - T_a + (\alpha - \eta_{el})GR_t] \left[ 1 - \exp\left(-\frac{A_c}{\dot{m}C_p R_{ov}}\right) \right] \quad (3)$$

$$\eta_{th} = \frac{\dot{q}_{th}}{G} \quad (4)$$

$$\dot{W}_{PV} = G\eta_{el} \quad (5)$$

$$\eta_{el} = \eta_{ref} \left[ 1 + \beta_{ref}(\bar{T}_c - T_{STC}) \right] \quad (6)$$

where  $T_a$  is ambient temperature,  $T_{eff}$  is effective air temperature,  $R_t$  is total thermal resistance at the top surface of the PVT collector,  $A_c$  is the area of PVT collector,  $\dot{m}$  is air mass flow rate,  $C_p$  is the specific heat of air,  $R_{ov}$  is overall thermal resistance,  $\eta_{ref}$  is electrical efficiency of the PV module under the standard condition,  $\beta_{ref}$  is the temperature coefficient,  $\bar{T}_c$  is the average cell temperature of the PV module, and  $T_{STC}$  is the temperature of the standard condition.

The total heat loss ( $\dot{q}_{loss}$ ) is composed of both convection and radiation heat loss, and it was given by:

$$\dot{q}_{loss} = \frac{T_{eff} - \bar{T}_c}{R_t} \quad (7)$$

where

$$T_{eff} = \frac{T_a R_{r,t} + T_{sky} R_{c,t}}{R_{r,t} + R_{c,t}} \quad (8)$$

$$R_t = \frac{R_{r,t} R_{c,t}}{R_{r,t} + R_{c,t}} \quad (9)$$

where  $T_{sky}$ ,  $R_{c,t}$ , and  $R_{r,t}$  are sky temperature, thermal resistance for convective heat transfer, and thermal resistance for radiative heat transfer, respectively.

The overall thermal resistance ( $R_{ov}$ ) used in Equations (2)–(4) was given by:

$$R_{ov} = R_t + R_f \quad (10)$$

where  $R_f$  is fluid thermal resistance between the PV module and flowing air in an air duct. A more detailed description of thermal resistance presented in the above equations was written in Section 2.2.

### 2.2. Thermal Resistance

This section describes the thermal resistance used in the mathematical model. The sky temperature ( $T_{sky}$ ) is obtained using the following empirical equation [37,38]:

$$T_{sky} = 0.0552T_a^{1.5} \quad (11)$$

With the above equation, the radiative thermal resistance ( $R_{r,t}$ ) can be calculated by using the following equation [39]:

$$R_{r,t} = \frac{1}{h_{r,t}} = \frac{1}{\varepsilon\sigma(\bar{T}_c^2 + T_{sky}^2)(\bar{T}_c + T_{sky})} \quad (12)$$

where  $h_{r,t}$ ,  $\varepsilon$ , and  $\sigma$  are the radiative heat transfer coefficient, the emissivity of the PV module, and Stefan–Boltzmann constant ( $5.67 \times 10^{-8} \text{ W/m}^2\text{K}^4$ ), respectively.

The convective thermal resistance ( $R_{c,t}$ ) at the top surface of the collector is given by [38,40,41]:

$$R_{c,t} = \frac{1}{h_{c,t}} = \frac{1}{3.0\dot{V}_{wind} + 2.8} \quad (13)$$

The fluid thermal resistance ( $R_f$ ) is calculated using the following equation:

$$R_f = \frac{D_h}{k(Nu)} \quad (14)$$

where  $D_h$  and  $k$  are the hydraulic diameter and the thermal conductivity of air, respectively. The Nusselt number in an air channel containing triangle-shaped obstacles was taken from the numerical results presented in Ref. [42]. It can be expressed as:

$$Nu = 0.2899Re^{0.6828}(e_{rib}/H)^{1.6939}(l_{rib}/e_{rib})^{-0.0221}(p_{rib}/e_{rib})^{0.0563} \exp[0.5604 \{\ln(e_{rib}/H)\}^2] \exp[-0.0159\{\ln(l_{rib}/e_{rib})\}^2] \exp[-0.0122\{\ln(p_{rib}/e_{rib})\}^2] \quad (15)$$

where  $e_{rib}$ ,  $l_{rib}$ , and  $p_{rib}$  are the height, length, and pitch of the triangle-shaped obstacle, respectively. The  $H$  is the height of the air channel of the PVT collector.

The Nusselt number for a conventional PVT collector was obtained using the following equation [16,36]:

$$Nu_s = 0.023 Re^{0.8} Pr^{0.4} \quad (16)$$

### 2.3. Solution Process

In this study, the PVT collector performance was determined via the following solution process with the aforementioned equations:

- First, the cell temperature of the PVT collector was assumed to be 0.01 °C higher than the ambient temperature.
- Second, the thermal resistances were calculated with the assumed cell temperature.
- Third, electrical efficiency, thermal output, and total heat loss were obtained based on the calculated thermal resistances.
- Fourth, the left- and right-hand side terms in Equation (1) were compared.

The iterative calculation was performed for the above process if the error between the left- and right-hand side terms was greater than 1%, after adding 0.01 °C to the initial cell temperature until the error was less than 1%. Figure 2 presents the flow chart of the solution process.

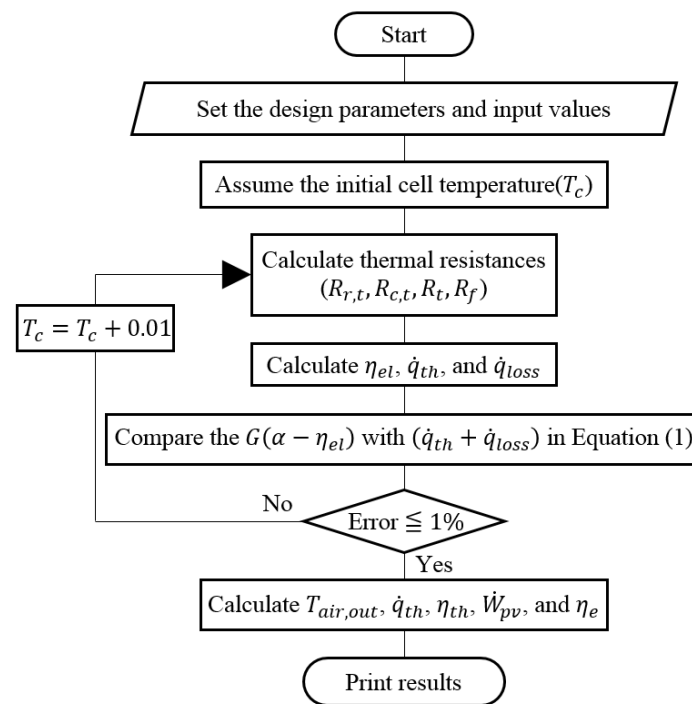


**Figure 2.** Flow chart of the solution process.

### 3. Energy and Exergy Analysis

#### 3.1. Energy Analysis

The energy performance of the PVT collector was evaluated including the outlet air temperature, thermal output, thermal efficiency, electrical power output, electrical efficiency, overall energy output, and overall energy efficiency. The outlet air temperature, thermal output, thermal efficiency, electrical power output, and electrical efficiency were obtained from Equations (2), (3), (4), (5), and (6), respectively.

From an economic perspective, electrical energy is generally considered to be of higher quality than thermal energy. Thus, the PVT collectors are generally assessed based on their overall energy output and efficiency by converting their electrical efficiency into their equivalent thermal efficiency, and it can be obtained by using the following equations [17,43–46].

$$\dot{q}_{ov} = \dot{q}_{th} + \frac{\dot{W}_{PV}}{C_f} \quad (17)$$

$$\eta_{ov} = \eta_{th} + \frac{\eta_{el}}{C_f} \quad (18)$$

where  $C_f$  is the conversion factor for the equivalent thermal efficiency. In this research, a value of 0.38 was assumed for the conversion factor, similar to other research [43,45–48].

#### 3.2. Exergy Analysis

Exergy is the maximum work that can be retrieved from a system that is in reversible equilibrium with its environment. For an air-cooled PVT collector, the exergy balance can be expressed as follows [14,20,49,50]:

$$\sum \dot{E}x_{in} - \sum \dot{E}x_{out} = \sum \dot{E}x_{dest} \quad (19)$$

or

$$\sum \dot{E}x_{in} - \sum (\dot{E}x_{PV} + \dot{E}x_{th}) = \sum \dot{E}x_{dest} \quad (20)$$

where

$$\dot{E}x_{in} = G \left[ 1 - \frac{4}{3} \left( \frac{T_a}{T_s} \right) + \frac{1}{3} \left( \frac{T_a}{T_s} \right)^4 \right] \quad (21)$$

$$\dot{E}x_{PV} = G\eta_{ref} \left[ 1 + \beta_{ref} (\bar{T}_c - T_{STC}) \right] \quad (22)$$

$$\dot{E}x_{th} = \dot{q}_{th} \left[ 1 - \frac{T_a + 273}{T_{air,out} + 273} \right] \quad (23)$$

$$\dot{E}x_{PVT} = \dot{E}x_{PV} + \dot{E}x_{th} \quad (24)$$

in which  $\dot{E}x_{in}$ ,  $\dot{E}x_{out}$ ,  $\dot{E}x_{dest}$ ,  $\dot{E}x_{PV}$ ,  $\dot{E}x_{th}$ ,  $\dot{E}x_{PVT}$ , and  $T_s$  are the total inflow exergy, total outflow exergy, destruction of exergy, electrical exergy, thermal exergy, exergy output of the air-cooled PVT collector, and temperature of the sun (5777 K), respectively [20,49].

An exergy efficiency is the ratio of the net output exergy to the total inflow exergy, and it is given by [14,20,51]:

$$\eta_{ex} = \frac{\dot{E}x_{out}}{\dot{E}x_{in}} \quad (25)$$

#### 4. Validation

In the present study, the mathematical model for the PVT collector with triangle-shaped obstacles was validated using experimental values reported in the previous research. The PVT collector included a monocrystalline-type PV module, which is a commercially available product, and an air channel containing triangular obstacles. Figures 3 and 4 show a schematic of the PVT collector with triangle-shaped obstacles and a side view of the collector used in the experiment, respectively. The experiment was conducted on the actual weather condition in Busan, Korea. During the experiment, the fan installed at the inlet side of the PVT collector maintained a constant air mass flow rate. The design parameters of the PVT collector used in the previous experiment as well as the numerical model for this study during the validation setup are given in Table 1. A more detailed description of the experimental method and conditions can be found in the previously published paper [30].

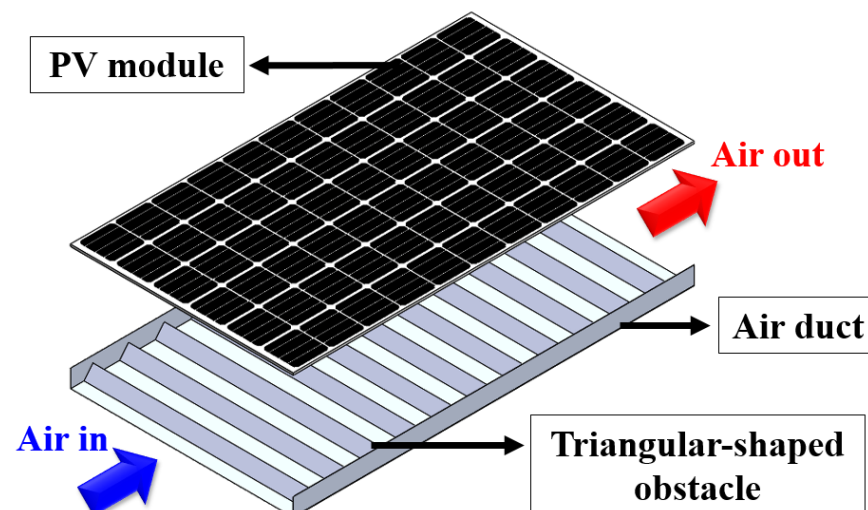


**Figure 3.** Schematic of the air-cooled PVT collector with triangle-shaped obstacles (reprinted/adapted with permission from Ref. [30]. Copyright 2020, Elsevier Ltd.).

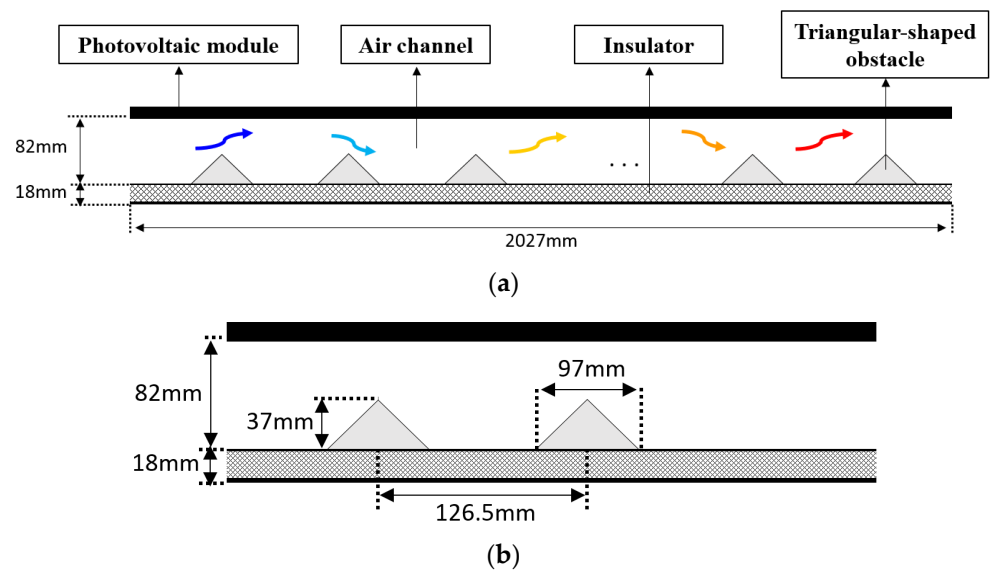


**Figure 4.** Side view of the air-cooled PVT collector with triangle-shaped obstacles: (a) side view and (b) dimensions (reprinted/adapted with permission from Ref. [30]. Copyright 2020, Elsevier Ltd.).

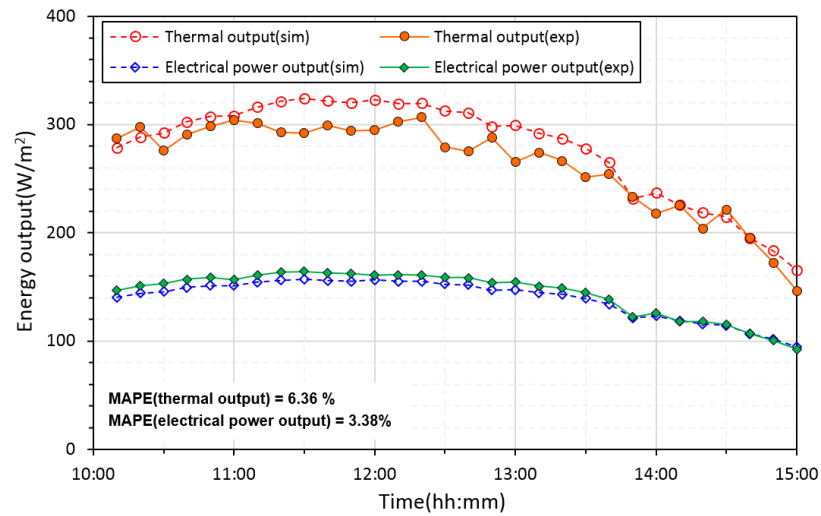
**Table 1.** Design parameters of the air-cooled PVT collector with triangular obstacles.

Parameter	Value
Electrical efficiency at standard test condition (%), $\eta_{ref}$	17.37
Temperature coefficient (%/°C), $\beta_{ref}$	−0.41
Temperature of the standard test condition (°C), $T_{STC}$	25
Absorption coefficient of the PV module (-), $\alpha$	0.85
Emissivity of the PVT collector, $\epsilon$	0.88
Length of the air channel (mm), $L$	2027
Height of the air channel (mm), $H$	83
Width of the air channel (mm), $w$	1000
Height of a triangular obstacle (mm), $e_{rib}$	37
Length of a triangular obstacle (mm), $l_{rib}$	97
Pitch of a triangular obstacle (mm), $p_{rib}$	126.5
Area of the air-cooled PVT collector (m <sup>2</sup> ), $A_c$	2.027
Air flow rate (kg/m <sup>2</sup> s)	0.05527

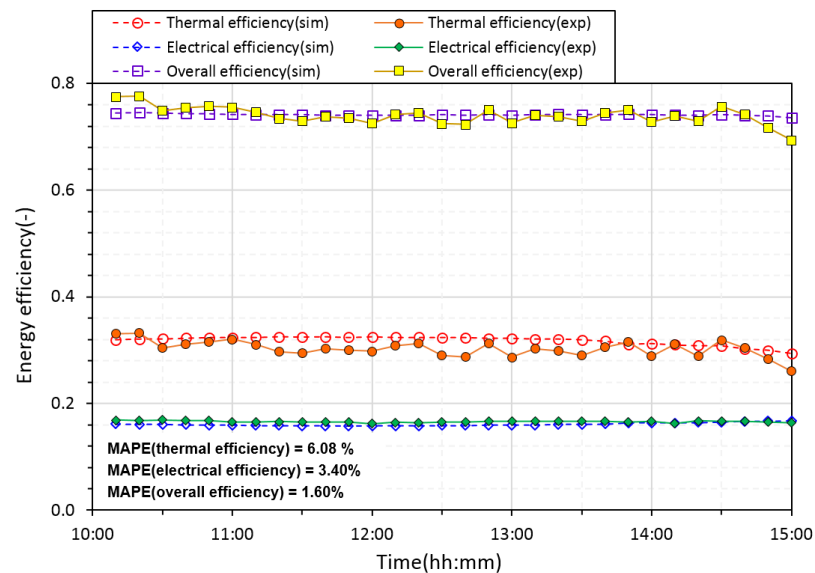
The weather conditions recorded in the previous study were used as input values to obtain the results of the simulation model. The mean absolute percentage error (MAPE) was used to compare the simulated results and experimental results. The MAPE was calculated using the following equations [17,52]:

$$MAPE (\%) = 100 \times \frac{\sum_{i=1}^n |(X_{sim,i} - X_{exp,i}) / X_{exp,i}|}{n} \quad (26)$$

Figure 5 shows the simulated results for energy output and efficiency compared with the corresponding experimental data obtained from Ref. [30]. The simulation results were found to be reasonably accurate in predicting the experimental results. The MAPE values were 6.36%, 3.38%, 6.08%, 3.40%, and 1.60% for thermal output, electrical power output, thermal efficiency, electrical efficiency, and overall efficiency, respectively.



(a)



(b)

**Figure 5.** Comparison between predicted values from the numerical model and experimental values: (a) energy output and (b) energy efficiency.

## 5. Methodology

The mathematical model developed and validated in this study was programmed and simulated in Matlab R2020a. The developed model was used to estimate the daily and annual performance of the PVT collector with and without triangle-shaped obstacles. The typical meteorological year weather data for Ulsan in Korea was used as the weather data. The annual incident solar radiation for Ulsan with different collector slopes is presented in Figure 6. The results showed that  $30.9^\circ$  is the optimum slope angle for the collector. Thus, the simulations of the PVT collector with and without triangle-shaped obstacles have been conducted with a slope angle of  $30.9^\circ$ . The design parameters used in the validation setup were employed for the simulations.

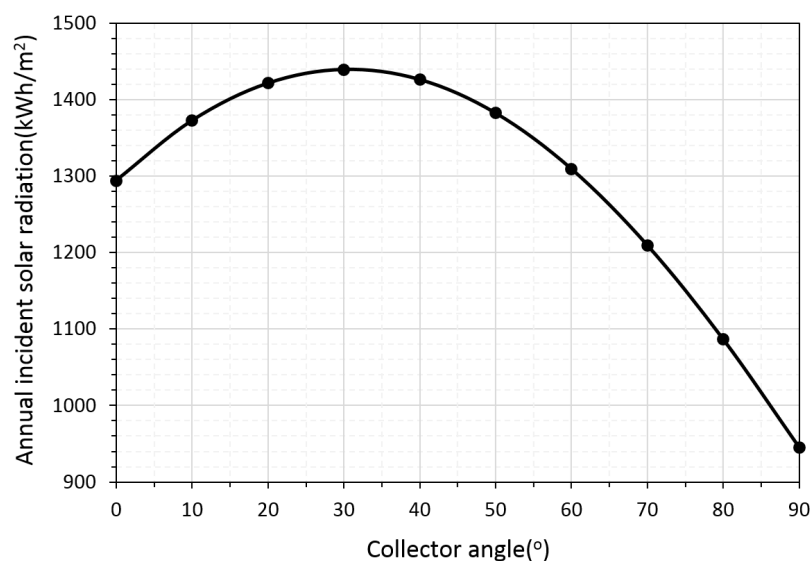


**Figure 6.** Annual incident solar radiation for Ulsan with different collector angles.

For daily and annual performance evaluation, the cell temperature, outlet air temperature, thermal output, thermal efficiency, electrical power output, electrical efficiency, overall energy output, overall energy efficiency, exergy output, and exergy efficiency have been observed. In the simulation model, temperatures, thermal and electrical outputs, and thermal and electrical efficiencies were obtained; the Equations (17), (18), (24), and (25) were then used to calculate the overall energy output, overall energy efficiency, exergy output, and exergy efficiency, respectively.

## 6. Results and Discussion

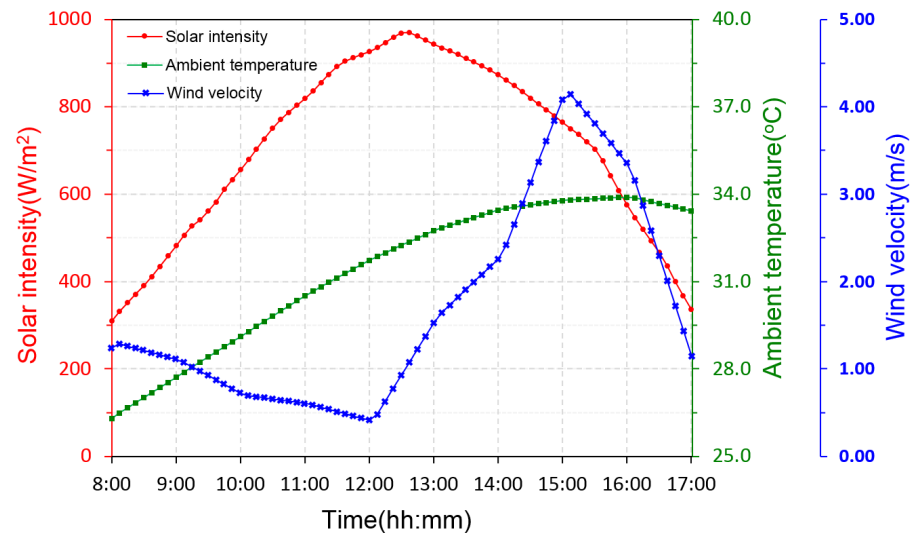
### 6.1. Daily Performance

The daily performance of the PVT collector with and without triangle-shaped obstacles was evaluated on a clear day (18 August). Figure 7 shows the weather conditions used to simulate the daily performance of the collector. Figure 8 presents the PV cell temperature and outlet air temperature for the PVT collector with and without triangle-shaped obstacles. The maximum cell temperature is found to be 61.2 °C for the PVT collector with triangle-shaped obstacles, while the conventional PVT collector shows 68.52 °C under the same weather conditions. The PVT collector with obstacles continuously exhibits a lower cell temperature than that of the conventional PVT collector because the triangle-shaped obstacles improve the heat transfer performance in an air channel of the collector. For the same reason, the outlet air temperature of the PVT collector with triangle-shaped obstacles shows higher values than those of the PVT collector without obstacles during the operation time.

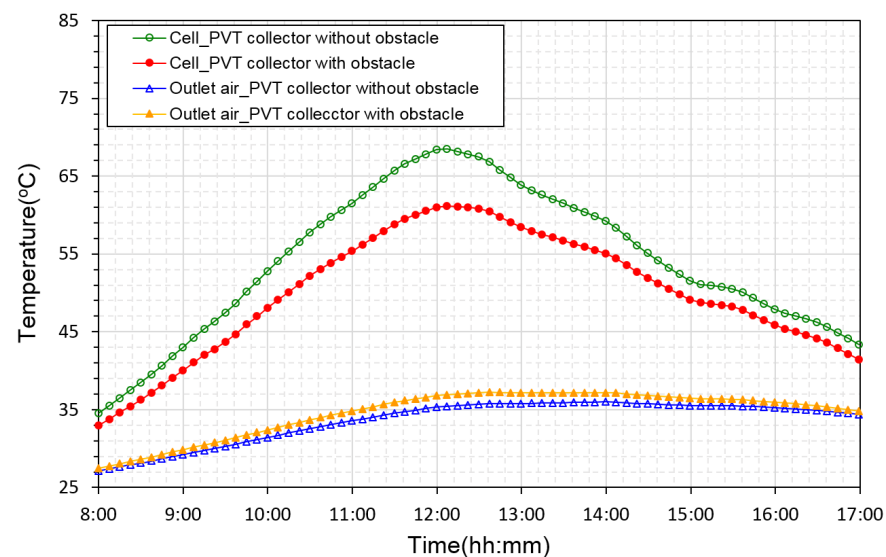
Figure 9 shows the thermal and electrical outputs of the PVT collectors. The maximum values of the thermal and electrical outputs are 199.15 W/m<sup>2</sup> and 129.69 W/m<sup>2</sup> for the conventional PVT collector and 281.58 W/m<sup>2</sup> and 133.78 W/m<sup>2</sup> for the collector with triangle-shaped obstacles. The results indicated that the installation of obstacles can improve the collector's thermal and electrical outputs.

Figure 10 depicts the thermal and electrical efficiencies of the PVT collector with and without triangle-shaped obstacles. The thermal efficiency varies from 12.5–21.51% with a mean value of 17.08% for the conventional PVT collector and from 19.12–30.35% with a mean value of 24.73% for the PVT collector with triangle-shaped obstacles during the operation time. As expected, the PVT collector with triangle-shaped obstacles had higher thermal efficiency than the conventional PVT collector. Electrical efficiency was in the range of 14.27–16.69% for the conventional PVT collector, with an average value of 15.30%, while that of the PVT collector with triangle-shaped obstacles ranges from 14.79% to 16.80% with an average value of 15.59%. The electrical efficiency of the PVT

collector with triangle-shaped obstacles shows consistently higher values than that of the conventional PVT collector during the operation time owing to the lower cell temperature. Additionally, it was observed that the addition of the obstacle can lead to an enhancement of the collector's electrical output as well as thermal output.



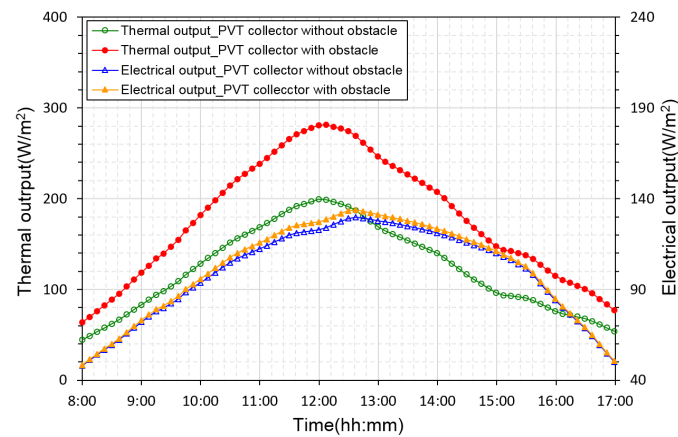
**Figure 7.** Variations in the solar intensity, ambient temperature, and wind velocity used to simulate daily performance.



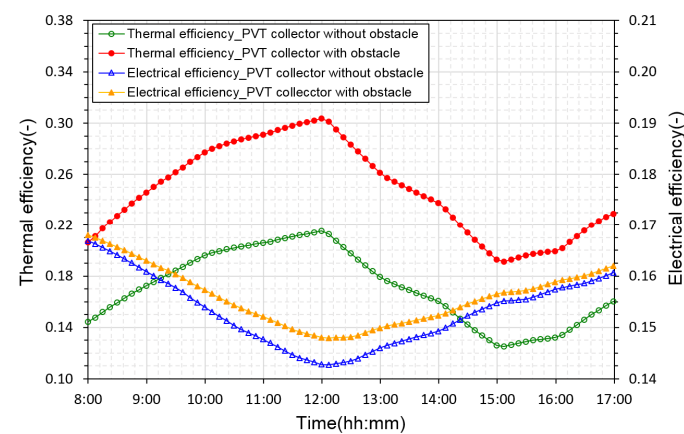
**Figure 8.** Variations in the PV cell and outlet air temperature for PVT collectors with and without triangle-shaped obstacles.

Figure 11 presents the overall energy output and efficiency. The overall energy output varies from 171.52–531.20 W/m<sup>2</sup> for the conventional PVT collector, with an average value of 384.97 W/m<sup>2</sup>, while the overall energy output varies from 191.55–625.63 W/m<sup>2</sup> with an average value of 445.76 W/m<sup>2</sup> for the PVT collector with triangle-shaped obstacles. The overall energy efficiency is in the range of 50.41–57.22% for the conventional PVT collector and 57.44–66.54% for the PVT air collector with triangle-shaped obstacles. The daily average overall energy efficiencies are found to be 54.47% for the conventional PVT collector and 62.83% for the PVT collector with triangle-shaped obstacles. The result showed that adding the obstacle can increase the daily overall energy efficiency of the collector by approximately

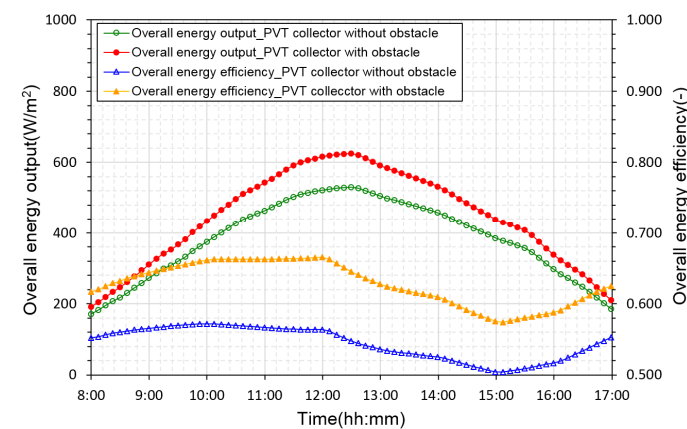
15.35%. Moreover, it was seen that the overall energy efficiency obtained in this study was higher than that of similar PVT collectors without triangle-shaped obstacles [17,41,51,53,54].



**Figure 9.** Variations in the thermal and electrical outputs for PVT collectors with and without triangle-shaped obstacles.



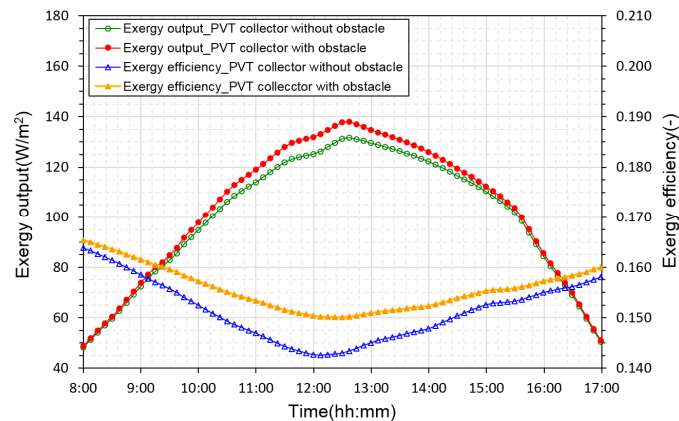
**Figure 10.** Variations in the thermal and electrical efficiencies for PVT collectors with and without triangle-shaped obstacles.



**Figure 11.** Variation in the overall energy output and efficiency for PVT collectors with and without triangle-shaped obstacles.

Figure 12 depicts the exergy output and efficiency of the PVT collectors. The PVT collector with triangle-shaped obstacles generated more exergy during operation than

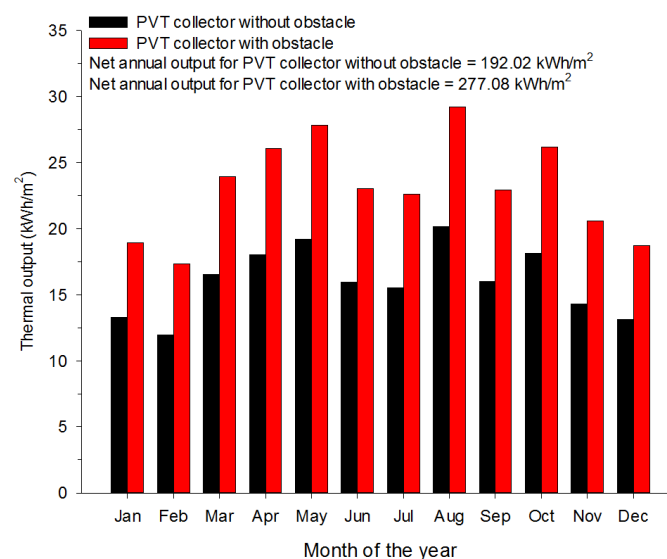
the conventional PVT collector. The exergy efficiency varied from 14.25–16.39% with an average value of 15.13% for the conventional PVT collector and 15.01–16.54% with an average value of 15.57% for the PVT collector with triangle-shaped obstacles, respectively. The daily exergy efficiency increased by 2.91% as a result of the installation of the obstacle, and the results clearly showed that the installation of the obstacles can improve the exergy performance of the collector as well as the energy performance. It was also found that the exergy efficiency confirmed in the present work was higher than that of the conventional PVT collectors without triangle-shaped obstacles [14,51,55].



**Figure 12.** Variation in the exergy output and efficiency for PVT collectors with and without triangle-shaped obstacles.

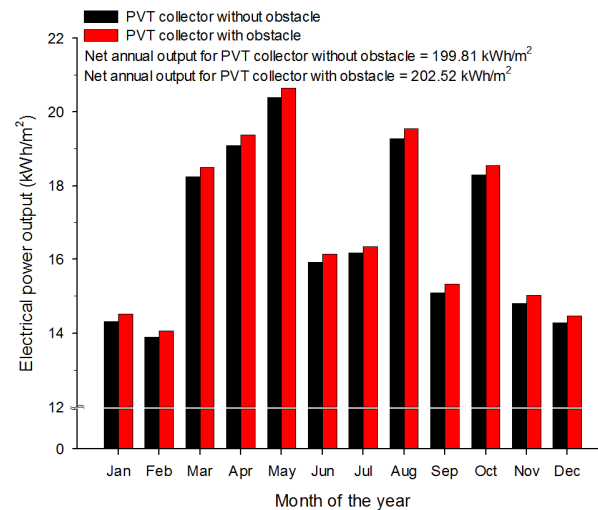
## 6.2. Annual Performance

Figure 13 shows the monthly thermal outputs of the PVT collectors with and without triangle-shaped obstacles. The monthly thermal outputs vary from 11.95–20.13 kWh/m<sup>2</sup> for the conventional PVT collector and 17.30–29.17 kWh/m<sup>2</sup> for the PVT collector with triangle-shaped obstacles, respectively. The net annual thermal outputs are found to be 192.02 kWh/m<sup>2</sup> and 277.08 kWh/m<sup>2</sup>, for the PVT collector without obstacles and the PVT collector with triangle-shaped obstacles, respectively. From the results, it was observed that the net annual thermal output of the collector can be improved by 44.3% as a result of the addition of triangle-shaped obstacles.



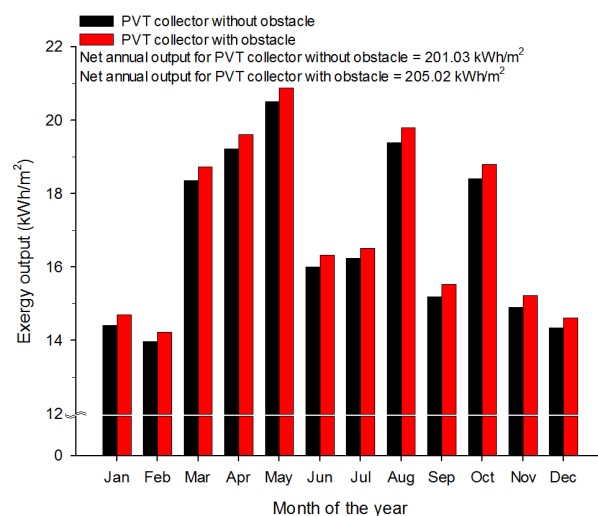
**Figure 13.** Monthly variation in thermal outputs for PVT collectors with and without triangle-shaped obstacles.

Figure 14 presents the monthly electrical power output. The monthly electrical power outputs are in the range of 13.89–20.40 kWh/m<sup>2</sup> with a net annual electrical output of 199.81 kWh/m<sup>2</sup> for the conventional PVT collector and 14.07–20.65 kWh/m<sup>2</sup> with a net annual electrical output of 202.52 kWh/m<sup>2</sup> for the PVT collector with triangle-shaped obstacles. The results confirmed that the triangle-shaped obstacles can provide an increase of 1.36% in the net annual electrical power output of the collector. Additionally, it was evident that installing triangle-shaped obstacles in the air-cooled PVT collector can improve annual thermal and electrical energy outputs.



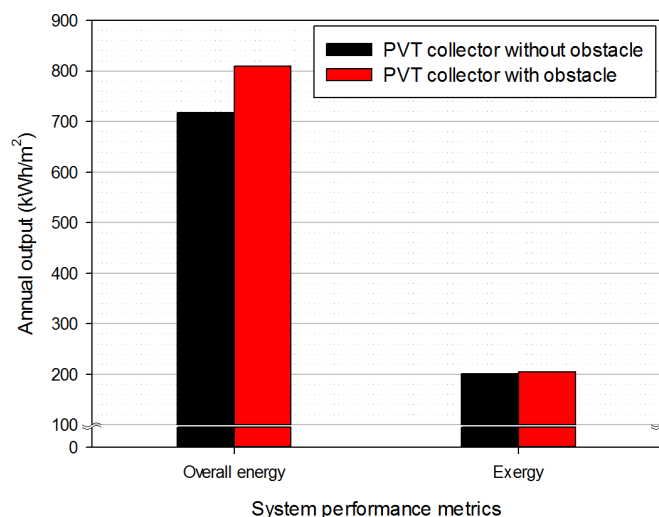
**Figure 14.** Monthly variation in electrical output for PVT collectors with and without triangle-shaped obstacles.

Figure 15 shows the monthly exergy outputs for the PVT collector with and without triangle-shaped obstacles. The exergy outputs vary from 13.97–20.51 kWh/m<sup>2</sup> for the conventional PVT collector and 14.23–20.88 kWh/m<sup>2</sup> for the PVT collector with triangle-shaped obstacles, respectively. The results showed that the PVT collector with triangle-shaped obstacles can achieve higher exergy output than that of the conventional PVT collector in all months owing to the improvement of both the thermal and electrical energy outputs. The net annual exergy outputs were found to be 201.03 kWh/m<sup>2</sup> for the conventional PVT collector and 205.02 kWh/m<sup>2</sup> for the PVT collector with triangle-shaped obstacles.



**Figure 15.** Monthly variation in exergy output for PVT collectors with and without triangle-shaped obstacles.

Figure 16 shows the net annual overall energy and exergy outputs. The net annual overall energy outputs are 717.83 kWh/m<sup>2</sup> for the conventional PVT collector and 810.01 kWh/m<sup>2</sup> for the PVT collector with triangle-shaped obstacles, respectively. From the figure, it could be confirmed that the annual overall energy and exergy outputs of the PVT collector can be improved by 12.84% and 1.98%, respectively, by the triangle-shaped obstacle.



**Figure 16.** Annual overall energy and exergy outputs for PVT collectors with and without triangle-shaped obstacles.

## 7. Conclusions

In the present work, a mathematical model of the air-cooled PVT collector containing triangle-shaped obstacles was developed based on the thermal circuit model and was validated with experimental results. The daily and annual performances of the PVT collector with and without triangle-shaped obstacles were investigated. Finally, the energy and exergy performance of the PVT collector with triangle-shaped obstacles compared to those of a PVT collector without the obstacles to confirm the influence of the triangle-shaped obstacles. The key findings are as follows:

- (1) From the daily operation, it was confirmed that the installation of triangle-shaped obstacles leads to a reduction in the cell temperature and an increase in the outlet air temperature of the air-cooled PVT collector.
- (2) The daily average thermal, electrical, and overall energy efficiencies were found to be 24.73%, 15.59%, and 62.83%, respectively, for the PVT collector with triangle-shaped obstacles, while those of the conventional PVT collector were 17.08%, 15.30%, and 54.47%, respectively. The daily overall efficiency could be improved by 15.35% as a result of the installation of obstacles.
- (3) The daily average exergy efficiency was 15.13% for the conventional PVT collector and 15.57% for the PVT collector with triangle-shaped obstacles. The presence of the obstacle leads to an increase of about 2.91% in the exergy efficiency of the collector.
- (4) The PVT collector with triangle-shaped obstacles could achieve about 44.3% and 1.36% more in the net annual thermal and electrical outputs, respectively, compared to those of the conventional PVT collector. In addition, the net annual overall energy output and exergy output of the PVT collector with triangle-shaped obstacles were found to be 12.84% and 1.98% greater than those of the conventional PVT collector, respectively.

The results found in this study clearly showed that the presence of triangular obstacles can improve the energy and exergy performance of the air-cooled PVT collector. Furthermore, the proposed air-cooled PVT collector presented a better performance in all of the daily, monthly, and annual energy and exergy performances. Thus, the feasibility of triangle-shaped obstacles was confirmed.

**Author Contributions:** Conceptualization, K.-H.C. and B.-H.A.; data curation, H.-U.C.; investigation, H.-U.C., K.-H.C. and B.-H.A.; methodology, H.-U.C.; software, H.-U.C. and B.-H.A.; validation, B.-H.A.; visualization, H.-U.C.; Writing—original draft, H.-U.C. and B.-H.A.; writing—review and editing, H.-U.C., K.-H.C. and B.-H.A. All authors have read and agreed to the published version of the manuscript.

**Funding:** This research received no external funding.

**Institutional Review Board Statement:** Not applicable.

**Informed Consent Statement:** Not applicable.

**Data Availability Statement:** Not applicable.

**Conflicts of Interest:** The authors declare no conflict of interest.

## Nomenclature

$A_c$	collector area ( $m^2$ )
$\dot{m}$	air mass flow rate ( $kg/s$ )
$C_p$	specific heat of air ( $J/kg\ K$ )
$D_h$	hydraulic diameter ( $m$ )
$G$	solar intensity ( $W/m^2$ )
$T$	temperature ( $^{\circ}C$ )
$T_{STC}$	temperature at the standard test condition ( $^{\circ}C$ )
$\bar{T}_c$	average temperature of the PV cell ( $^{\circ}C$ )
$T_{eff}$	effective air temperature ( $K$ )
$h$	heat transfer coefficient ( $W/m^2\ K$ )
$R$	thermal resistance ( $m^2\ K/W$ )
$R_{ov}$	overall thermal resistance ( $m^2\ K/W$ )
$\dot{V}_{wind}$	wind velocity ( $m/s$ )
$\dot{V}_{avg}$	average air velocity in an air channel ( $m/s$ )
$\dot{q}_{th}$	thermal output ( $W/m^2$ )
$\dot{q}_{ov}$	overall energy output ( $W/m^2$ )
$\dot{W}_{PV}$	electrical power output ( $W/m^2$ )
$\dot{E}_x$	exergy rate ( $W/m^2$ )
$k$	thermal conductivity of air ( $W/m\ K$ )
$H$	height of the air duct ( $mm$ )
$e_{rib}$	height of a triangle-shaped obstacle ( $mm$ )
$l_{rib}$	length of a triangle-shaped obstacle ( $mm$ )
$p_{rib}$	pitch of a triangle-shaped obstacle ( $mm$ )
$C_f$	conversion factor for the equivalent thermal efficiency (-)
$Nu$	Nusselt number (-)
$Re$	Reynolds number (-)
$Pr$	Prandtl number (-)
<b>Greek symbols</b>	
$\alpha$	absorptivity (-)
$\varepsilon$	emissivity (-)
$\sigma$	Stefan–Boltzmann constant ( $W/m^2\ K^4$ )
$\eta$	efficiency (-)
$\eta_{ov}$	overall energy efficiency (-)
$\eta_{ex}$	exergy efficiency (-)
$\eta_{ref}$	electrical efficiency at the standard test conditions (%)
$\beta_{ref}$	temperature coefficient ( $\%/^{\circ}C$ )

**Subscripts**

$\alpha$	ambient
$air$	air
$c$	convection
$r$	radiation
$t$	top surface
$in$	inflow
$out$	outflow
$dest$	destruction
$f$	fluid
$s$	sun
$sky$	sky
$th$	thermal
$el$	electrical
$PV$	PV module
$PVT$	PVT collector

**References**

1. Wolf, M. Performance Analyses of Combined Heating and Photovoltaic Power Systems for Residences. *Energy Convers. Manag.* **1976**, *16*, 79–90. [\[CrossRef\]](#)
2. Dupeyrat, P.; Ménézo, C.; Rommel, M.; Henning, H.M. Efficient Single Glazed Flat Plate Photovoltaic-Thermal Hybrid Collector for Domestic Hot Water System. *Sol. Energy* **2011**, *85*, 1457–1468. [\[CrossRef\]](#)
3. Jahromi, S.N.; Vadiée, A.; Yaghoubi, M. Exergy and Economic Evaluation of a Commercially Available PV/T Collector for Different Climates in Iran. *Energy Procedia* **2015**, *75*, 444–456. [\[CrossRef\]](#)
4. Aste, N.; Leonforte, F.; Del Pero, C. Design, Modeling and Performance Monitoring of a Photovoltaic-Thermal (PVT) Water Collector. *Sol. Energy* **2015**, *112*, 85–99. [\[CrossRef\]](#)
5. Kazem, H.A. Evaluation and Analysis of Water-Based Photovoltaic/Thermal (PV/T) System. *Case Stud. Therm. Eng.* **2019**, *13*, 100401. [\[CrossRef\]](#)
6. Hasan, H.A.; Sherza, J.S.; Mahdi, J.M.; Togun, H.; Abed, A.M.; Ibrahim, R.K.; Yaïci, W. Experimental Evaluation of the Thermoelectrical Performance of Photovoltaic-Thermal Systems with a Water-Cooled Heat Sink. *Sustainability* **2022**, *14*, 10231. [\[CrossRef\]](#)
7. Yan, B.; Wu, Q.; Chi, X.; Wu, C.; Luo, P.; Luo, Y.; Zeng, P. Numerical and Experimental Investigation of Photovoltaic/Thermal Systems: Parameter Analysis and Determination of Optimum Flow. *Sustainability* **2022**, *14*, 10156. [\[CrossRef\]](#)
8. Al-Waeli, A.H.A.; Sopian, K.; Kazem, H.A.; Yousif, J.H.; Chaichan, M.T.; Ibrahim, A.; Mat, S.; Ruslan, M.H. Comparison of Prediction Methods of PV/T Nanofluid and Nano-PCM System Using a Measured Dataset and Artificial Neural Network. *Sol. Energy* **2018**, *162*, 378–396. [\[CrossRef\]](#)
9. Fayaz, H.; Rahim, N.A.; Hasanuzzaman, M.; Rivai, A.; Nasrin, R. Numerical and Outdoor Real Time Experimental Investigation of Performance of PCM Based PVT System. *Sol. Energy* **2019**, *179*, 135–150. [\[CrossRef\]](#)
10. Xu, Z.; Kleinstreuer, C. Concentration Photovoltaic-Thermal Energy Co-Generation System Using Nanofluids for Cooling and Heating. *Energy Convers. Manag.* **2014**, *87*, 504–512. [\[CrossRef\]](#)
11. Al-Waeli, A.H.A.; Sopian, K.; Kazem, H.A.; Chaichan, M.T. Evaluation of the Electrical Performance of a Photovoltaic Thermal System Using Nano-Enhanced Paraffin and Nanofluids. *Case Stud. Therm. Eng.* **2020**, *21*, 100678. [\[CrossRef\]](#)
12. Hussain, M.I.; Lee, G.H.; Kim, J.T. A Comprehensive Performance Characterization of a Nanofluid-Powered Dual-Fluid Pv/t System under Outdoor Steady State Conditions. *Sustainability* **2021**, *13*, 3134. [\[CrossRef\]](#)
13. Sopian, K.; Yigit, K.S.; Liu, H.T.; Kakaç, S.; Veziroglu, T.N. Performance Analysis of Photovoltaic Thermal Air Heaters. *Energy Convers. Manag.* **1996**, *37*, 1657–1670. [\[CrossRef\]](#)
14. Agrawal, S.; Tiwari, G.N. Energy and Exergy Analysis of Hybrid Micro-Channel Photovoltaic Thermal Module. *Sol. Energy* **2011**, *85*, 356–370. [\[CrossRef\]](#)
15. Amori, K.E.; Abd-ALRaheem, M.A. Field Study of Various Air Based Photovoltaic/Thermal Hybrid Solar Collectors. *Renew. Energy* **2014**, *63*, 402–414. [\[CrossRef\]](#)
16. Farshchimonfared, M.; Bilbao, J.I.; Sproul, A.B. Channel Depth, Air Mass Flow Rate and Air Distribution Duct Diameter Optimization of Photovoltaic Thermal (PV/T) Air Collectors Linked to Residential Buildings. *Renew. Energy* **2015**, *76*, 27–35. [\[CrossRef\]](#)
17. Slimani, M.E.A.; Amirat, M.; Kurucz, I.; Bahria, S.; Hamidat, A.; Chaouch, W.B. A Detailed Thermal-Electrical Model of Three Photovoltaic/Thermal (PV/T) Hybrid Air Collectors and Photovoltaic (PV) Module: Comparative Study under Algiers Climatic Conditions. *Energy Convers. Manag.* **2017**, *133*, 458–476. [\[CrossRef\]](#)
18. Jin, G.L.; Ibrahim, A.; Chean, Y.K.; Daghigh, R.; Ruslan, H.; Mat, S.; Othman, M.Y.; Sopian, K. Evaluation of Single-Pass Photovoltaic-Thermal Air Collector with Rectangle Tunnel Absorber. *Am. J. Appl. Sci.* **2010**, *7*, 277–282. [\[CrossRef\]](#)

19. Hussain, F.; Othman, M.Y.H.; Yatim, B.; Ruslan, H.; Sopian, K.; Anuar, Z.; Khairuddin, S. An Improved Design of Photovoltaic/Thermal Solar Collector. *Sol. Energy* **2015**, *122*, 885–891. [[CrossRef](#)]
20. Fudholi, A.; Zohri, M.; Jin, G.L.; Ibrahim, A.; Yen, C.H.; Othman, M.Y.; Ruslan, M.H.; Sopian, K. Energy and Exergy Analyses of Photovoltaic Thermal Collector with  $\nabla$ -Groove. *Sol. Energy* **2018**, *159*, 742–750. [[CrossRef](#)]
21. Ahmad, E.Z.; Fazlizan, A.; Jarimi, H.; Sopian, K.; Ibrahim, A. Enhanced Heat Dissipation of Truncated Multi-Level Fin Heat Sink (MLFHS) in Case of Natural Convection for Photovoltaic Cooling. *Case Stud. Therm. Eng.* **2021**, *28*, 101578. [[CrossRef](#)]
22. Fudholi, A.; Sopian, K.; Othman, M.Y.; Ruslan, M.H.; Bakhtyar, B. Energy Analysis and Improvement Potential of Finned Double-Pass Solar Collector. *Energy Convers. Manag.* **2013**, *75*, 234–240. [[CrossRef](#)]
23. Othman, M.Y.; Yatim, B.; Sopian, K.; Abu Bakar, M.N. Performance Studies on a Finned Double-Pass Photovoltaic-Thermal (PV/T) Solar Collector. *Desalination* **2007**, *209*, 43–49. [[CrossRef](#)]
24. Kang, Z.; Lu, Z.; Song, G.; Yao, Q. A Numerical Study of Dual-Inlet Air-Cooled PV/T Solar Collectors with Various Airflow Channel Configurations. *Sustainability* **2022**, *14*, 9897. [[CrossRef](#)]
25. Fan, W.; Kokogiannakis, G.; Ma, Z. A Multi-Objective Design Optimisation Strategy for Hybrid Photovoltaic Thermal Collector (PVT)-Solar Air Heater (SAH) Systems with Fins. *Sol. Energy* **2018**, *163*, 315–328. [[CrossRef](#)]
26. Choi, H.U.; Choi, K.H. Performance Evaluation of PV/T Air Collector Having a Single-Pass Double-Flow Air Channel and Non-Uniform Cross-Section Transverse Rib. *Energies* **2020**, *13*, 2203. [[CrossRef](#)]
27. Özakin, A.N.; Kaya, F. Effect on the Exergy of the PVT System of Fins Added to an Air-Cooled Channel: A Study on Temperature and Air Velocity with ANSYS Fluent. *Sol. Energy* **2019**, *184*, 561–569. [[CrossRef](#)]
28. Fan, W.; Kokogiannakis, G.; Ma, Z.; Cooper, P. Development of a Dynamic Model for a Hybrid Photovoltaic Thermal Collector—Solar Air Heater with Fins. *Renew. Energy* **2017**, *101*, 816–834. [[CrossRef](#)]
29. Kim, S.M.; Kim, J.H.; Kim, J.T. Experimental Study on the Thermal and Electrical Characteristics of an Air-Based Photovoltaic Thermal Collector. *Energies* **2019**, *12*, 2661. [[CrossRef](#)]
30. Choi, H.U.; Kim, Y.B.; Son, C.H.; Yoon, J.I.; Choi, K.H. Experimental Study on the Performance of Heat Pump Water Heating System Coupled with Air Type PV/T Collector. *Appl. Therm. Eng.* **2020**, *178*, 115427. [[CrossRef](#)]
31. Choi, H.U.; Choi, K.H. Performance Evaluation of PVT Air Collector Coupled with a Triangular Block in Actual Climate Conditions in Korea. *Energies* **2022**, *15*, 4150. [[CrossRef](#)]
32. Yu, J.S.; Kim, J.H.; Kim, J.T. Effect of Triangular Baffle Arrangement on Heat Transfer Enhancement of Air-Type PVT Collector. *Sustainability* **2020**, *12*, 7469. [[CrossRef](#)]
33. Bambrook, S.M. Investigation of Photovoltaic/Thermal Air System to Create a Zero Energy House in Sydney. Ph.D. Thesis, University of New South Wales, Sydney, Australia, 2011.
34. Sproul, A.B.; Bilbao, J.I.; Bambrook, S.M. A Novel Thermal Circuit Analysis of Solar Thermal Collectors. In Proceedings of the 50th Annual Conference of the Australian Solar Energy Society, Melbourne, Australia, 2–4 December 2012.
35. Bilbao, J.I.; Sproul, A.B. Detailed PVT-Water Model for Transient Analysis Using RC Networks. *Sol. Energy* **2015**, *115*, 680–693. [[CrossRef](#)]
36. Bambrook, S.M.; Sproul, A.B. A Solvable Thermal Circuit for Modelling PVT Air Collectors. *Sol. Energy* **2016**, *138*, 77–87. [[CrossRef](#)]
37. Ong, K.S. Thermal Performance of Solar Air Heaters: Mathematical Model and Solution Procedure. *Sol. Energy* **1995**, *55*, 93–109. [[CrossRef](#)]
38. Tonui, J.K.; Tripanagnostopoulos, Y. Air-Cooled PV/T Solar Collectors with Low Cost Performance Improvements. *Sol. Energy* **2007**, *81*, 498–511. [[CrossRef](#)]
39. Cengel, Y.A.; Ghajar, A.J. *Heat and Mass Transfer (SI Unit)*, 4th ed.; McGraw-Hill: London, UK, 2011.
40. Aste, N.; Chiesa, G.; Verri, F. Design, Development and Performance Monitoring of a Photovoltaic-Thermal (PVT) Air Collector. *Renew. Energy* **2008**, *33*, 914–927. [[CrossRef](#)]
41. Sarhaddi, F.; Farahat, S.; Ajam, H.; Behzadmehr, A.; Mahdavi Adeli, M. An Improved Thermal and Electrical Model for a Solar Photovoltaic Thermal (PV/T) Air Collector. *Appl. Energy* **2010**, *87*, 2328–2339. [[CrossRef](#)]
42. Choi, H.U.; Choi, K.H. CFD Analysis on the Heat Transfer and Fluid Flow of Solar Air Heater Having Transverse Triangular Block at the Bottom of Air Duct. *Energies* **2020**, *13*, 1099. [[CrossRef](#)]
43. Huang, B.H.; Lin, T.H.; Hung, W.C.; Sun, F.S. Performance evaluation of solar photovoltaic/thermal systems. *Sol. Energy* **2001**, *70*, 443–448. [[CrossRef](#)]
44. Tiwari, A.; Sodha, M.S. Parametric Study of Various Configurations of Hybrid PV/Thermal Air Collector: Experimental Validation of Theoretical Model. *Sol. Energy Mater. Sol. Cells* **2007**, *91*, 17–28. [[CrossRef](#)]
45. Kumar, R.; Rosen, M.A. Performance Evaluation of a Double Pass PV/T Solar Air Heater with and without Fins. *Appl. Therm. Eng.* **2011**, *31*, 1402–1410. [[CrossRef](#)]
46. Mojumder, J.C.; Ong, H.C.; Chong, W.T.; Shamshirband, S.; Abdullah-Al-Mamoon Application of Support Vector Machine for Prediction of Electrical and Thermal Performance in PV/T System. *Energy Build.* **2016**, *111*, 267–277. [[CrossRef](#)]
47. Agrawal, B.; Tiwari, G.N. Optimizing the Energy and Exergy of Building Integrated Photovoltaic Thermal (BIPVT) Systems under Cold Climatic Conditions. *Appl. Energy* **2010**, *87*, 417–426. [[CrossRef](#)]
48. Sardarabadi, M.; Passandideh-Fard, M.; Zeinali Heris, S. Experimental Investigation of the Effects of Silica/Water Nanofluid OnPV/T (Photovoltaic Thermal Units). *Energy* **2014**, *66*, 264–272. [[CrossRef](#)]

49. Tiwari, A.; Dubey, S.; Sandhu, G.S.; Sodha, M.S.; Anwar, S.I. Exergy Analysis of Integrated Photovoltaic Thermal Solar Water Heater under Constant Flow Rate and Constant Collection Temperature Modes. *Appl. Energy* **2009**, *86*, 2592–2597. [[CrossRef](#)]
50. Ibrahim, A.; Fudholi, A.; Sopian, K.; Othman, M.Y.; Ruslan, M.H. Efficiencies and Improvement Potential of Building Integrated Photovoltaic Thermal (BIPVT) System. *Energy Convers. Manag.* **2014**, *77*, 527–534. [[CrossRef](#)]
51. Sarhaddi, F.; Farahat, S.; Ajam, H.; Behzadmehr, A. Exergetic Performance Assessment of a Solar Photovoltaic Thermal (PV/T) Air Collector. *Energy Build.* **2010**, *42*, 2184–2199. [[CrossRef](#)]
52. Jarimi, H.; Abu Bakar, M.N.; Othman, M.; Din, M.H. Bi-Fluid Photovoltaic/Thermal (PV/T) Solar Collector: Experimental Validation of a 2-D Theoretical Model. *Renew. Energy* **2016**, *85*, 1052–1067. [[CrossRef](#)]
53. Amori, K.E.; Taqi Al-Najjar, H.M. Analysis of Thermal and Electrical Performance of a Hybrid (PVT) Air Based Solar Collector for Iraq. *Appl. Energy* **2012**, *98*, 384–395. [[CrossRef](#)]
54. Senthilraja, S.; Gangadevi, R.; Marimuthu, R.; Baskaran, M. Performance Evaluation of Water and Air Based PVT Solar Collector for Hydrogen Production Application. *Int. J. Hydrog. Energy* **2020**, *45*, 7498–7507. [[CrossRef](#)]
55. Joshi, A.S.; Tiwari, A. Energy and Exergy Efficiencies of a Hybrid Photovoltaic-Thermal (PV/T) Air Collector. *Renew. Energy* **2007**, *32*, 2223–2241. [[CrossRef](#)]